Journal of
Nanoscience and Nanotechnology
Vol. 12, 8546–8553, 2012

Strain in Atomistic Models of Nanocrystalline Clusters

Alberto Leonardi[1,*], Matteo Leoni[1], Mo Li[2], and Paolo Scardi[1]

[1] *Department of Materials Engineering and Industrial Technologies, University of Trento, via Mesiano 77, I-38123, Trento, Italy*
[2] *Georgia Institute of Technology, Atlanta, USA*

Strain, as an easy and clearly defined concept in continuum mechanics, has no direct counterpart in atomistic models. Existing methods, relying on the concept of atomic coordination number, do not provide a complete description of volumetric and deviatoric strains across metallic nanocrystalline microstructures. To overcome those limitations a new method is proposed: the Voronoi Cell deformation (VCD) fully accounts for the local geometry and provides a description of the strain field independent of the atomic coordination. As a typical case of study, a large atomic cluster of 200 Al grains (ca 2 million atoms) and overall size of 33 cubic nanometres was considered.

Keywords: Strain at the Atomic Level, Nano-Polycrystalline Cluster, Microstrain, Voronoi Tessellation.

RESEARCH ARTICLE

1. INTRODUCTION

Atomistic modelling is increasingly employed to study properties and behaviour of materials under different conditions.[1] This is particularly valuable in the field of nanostructured materials where the microstructures can be created using space filling models[2,3] and then simulated by Molecular Dynamics (MD). Although results do not always match those of traditional experiments, this approach is informative and can most frequently capture the main features of the physical phenomena of interest.[4–7] The limited extension of the time scale commonly accessible to MD simulations penalizes some applications, like those concerning plasticity, but is perfectly adequate to represent thermal and elastic properties.

A major task is extracting models of behaviour compatible both with the macroscopic observation and with the MD scale. Strain, for example, is not properly defined at the atomic level because the traditional definition, based on continuum mechanics, does not apply to discrete systems on the atomic level. The complexity is even larger if atomic vibrations are to be considered as well.

Among the available methods, Neighbours Analysis (NA) studies the local geometrical arrangement of neighbours to detect structural features at the atomic level.[8,9] NA is a powerful tool to identify defects and phases in large systems, but is intrinsically unable to provide strain values. Therefore, NA is complemented by methods to calculate local pressure and stress,[10–12] as those properties are directly related to the energy of each atom, with no need to define or calculate strains.

More recently, methods have been proposed to compute the local atomic strain by comparing the arrangement of neighbours with respect to a perfect reference structure.[13,14] A major drawback is the impossibility to deal with strongly deformed structures, where atoms may not be fully coordinated. To overcome this limitation we propose the Voronoi Cell Deformation (VCD) method. Based on Voronoi Tessellation, the VCD avoids the somehow arbitrary concept of cut-off radius, required by existing methods.[13,14] Moreover, as it makes no reference to the atomic coordination, the VCD can be used across heavily defected regions as well as in the core on nanostructured domains.

2. METHODS

2.1. Molecular Dynamics Simulation

A nano-polycrystalline aluminium microstructure was created by randomly placing 200 centres in a box of 323.96 Å side length, using a homogeneous Poisson point process with parameter $\lambda = 1$.[15–17] Cells were identified in the box using Voronoi Tessellation and considering Periodical Boundary Conditions. This microstructure was then evolved by an inverse Monte Carlo method (Constrained Voronoi Tessellation[18]) to obtain a lognormal grain-size distribution of rounded grains.

Each cell was filled with a randomly oriented ideal *fcc* structure (Al unit cell parameter, $a_0 = 4.0495$ Å); atoms

*Author to whom correspondence should be addressed.

1533-4880/2012/12/8546/008 doi:10.1166/jnn.2012.6807

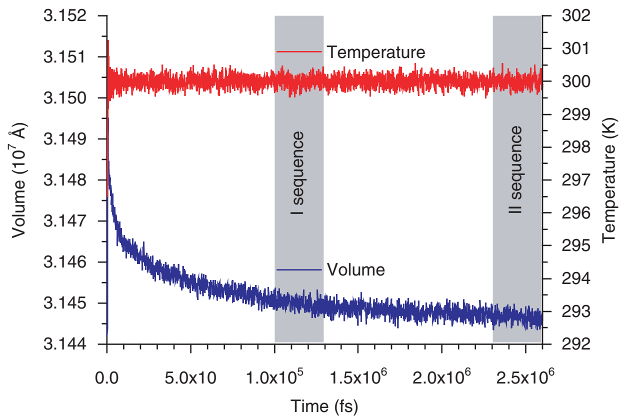

Fig. 1. Fluctuation of temperature and volume of the cluster during the equilibration process.

closer than 85% of the minimum distance in the *fcc* structure (a_0/sqrt(2)) were clipped as suggested in Ref. [19].

The starting crystalline microstructure was equilibrated at 300 K via the LAMMPS code[20] using the Embedded Atom Method (EAM)[21] and the Al potential of Jacobson, Norskov and Puska.[22] Two independent analyses were done respectively at 1 ns and at 2.3 ns since the beginning of the simulation (Fig. 1). At both times, 150 frames of the microstructure were sampled with a time interval of 2 ps, chosen to achieve full independency of the positions from thermal vibrations (other approaches are possible[13,23]). The atomic positions were averaged over the 150 frames to obtain models free of any dynamic strain contribution.

2.2. Strain at the Atomic Level

In solid mechanics, the local deformation is expressed by a normalized gradient tensor under the continuum approximation. This assumption is not valid in MD simulations, as the atomistic nature of matter is intrinsically discrete.

A reference configuration is needed to define the local strain. If the whole un-deformed microstructure is known, the local strain matrix can be directly computed from the minimization of the squared difference between the analyzed and the ideally deformed structures.[24] When the reference is unknown or have no physical meaning (e.g., close to the interface boundary zones in a polycrystalline system), a local crystallographic structure can be taken in place of the global one.

Two methods have been recently introduced to compute the strain matrix by comparing the arrangement of the neighbours with respect to the ideal local configuration. Both start by finding the neighbours and assigning them a specific order. Then, the method of Stukowsky et al. involves a linear least-square fitting of a strain matrix to transform the ideal structure into the observed (deformed) one.[13] As an alternative, the Crystallography Cell Deformation method (CCD)[14] estimates the significant geometric deformation of the local structure by identifying the principal crystallographic axes and lengths. Hence, the strain matrix is built by computing the direct and cross deformation coefficients.

Those methods are characterised by three principal features:

(i) neighbours are identified by considering an arbitrary cut-off radius.

(ii) deformation is computed by exploiting some topological properties of the local structure (e.g., symmetry).

(iii) deformation at the atomic level is linked to the arrangement of the whole set of near neighbours and so a fully coordinated structure is needed.

Those assumptions, unfortunately, limit the applicability of the corresponding methods and in particular do not allow the strain in the core of the deformation field to be computed.

2.2.1. *The Voronoi Cell Deformation Method* (*VCD*)

The Voronoi Tessellation (VT) method is a suitable tool to investigate the arrangement of the neighbours.[25]

As shown in Figure 2, each atom is the generator of a Voronoi Cell (VC) dual to the neighbours' arrangement. The geometric properties of the VC can be therefore analysed in place of the unit crystal structure. As a matter of fact, the strain at the atomic level affects the VC geometry, and thus the moments of mass. If the density of mass is assumed uniform in space, the moments of mass can be replaced by the moments of volume (see Appendix A).

The strains at the atomic level along the principal directions are easily estimated by the ratio of the principal inertia of the deformed and reference structures. Linking the inertia values of the VCs to the equivalent parallelepiped solids, the three stretch ratios ($0 < \lambda < \infty$) can be fully defined. From them, the strain can be computed as:

$$\varepsilon = \frac{1}{k}(\lambda^k - 1) \tag{1}$$

where $\kappa = 1$ or $\kappa = 2$ allow, respectively, the engineering and Lagrange strain to be obtained. In the end, the strain matrix can be written in terms of the principal strain associated to the principal inertia.

The space-filling nature of the VT ensures the congruence of the resulting strain values. The volumetric strain at the atomic level can be measured directly from the first moment of mass or it can be computed by the product of the stretch ratios. In both cases the macro-scale deformation is consistent with the local deformation. Therefore, a discrepancy is detected between measured and real crystal deformation, which is due to the assumption of the equivalent inertia of a parallelepiped solid involved.

A variant of the VCD can be introduced to better take the geometric positions of the neighbours into account: the VT is again employed to identify the neighbours according to the procedure proposed by O'Keeffe.[26] The strain

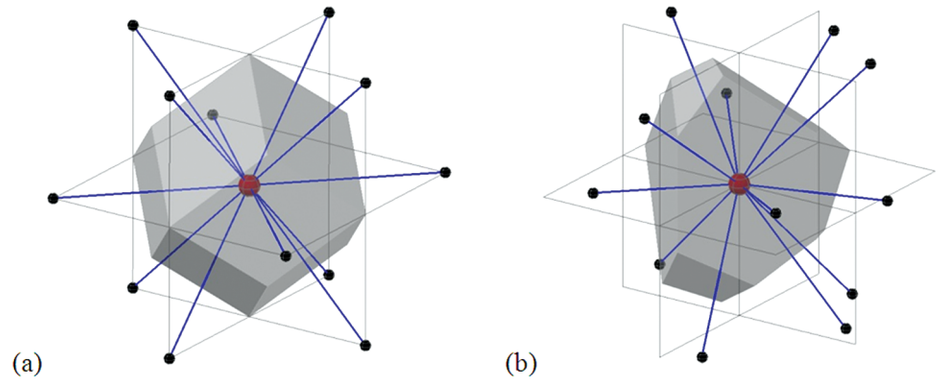

Fig. 2. Voronoi tessellations for a perfect (a) and for a distorted (b) fcc structure.

at the atomic level is then computed from the fluctuation of the moments of mass (see Appendix B). Contrary to the above, the atomistic nature is fully exploited here: the mass is therefore considered as concentrated at each atom position (Voronoi moment of mass Cell Deformation method (VmmCD)). Without losing in generality, each atomic position is assigned a unitary mass: in agreement with the geometric nature of the deformation, each Voronoi neighbour contributes to the local structure with a magnitude related to the size of the linked VC face. The point masses need thus being weighted by the relative VC-side surface area (weighted VmmCD method).

2.2.2. *The Evolutional Voronoi Cell Deformation Method* (*eVCD*)

The VCD method solves the strain matrix by assuming a link between inertia values of the VCs and of the equivalent parallelepipeds. This is true only in some crystal structure, e.g., the simple cubic. An evolutional algorithm has to be used to avoid any link to a specific crystallographic VC shape.

The principal directions, the inertia and the true volumetric deformation at the atomic level were computed on a given cluster by using the VCD method. Starting from applied deformations (λ_i, λ_j and λ_k), the agreement of the deformed reference structure with the configuration detected in the model is evaluated by a likelihood function χ^2:

$$\chi^2 = \sum_{i=1}^{3} \left(I_i^{\mathrm{MODEL}} - I_i^{\mathrm{REAL}} \right)^2 \qquad (2)$$

which is equal to the sum of the squared difference between the inertia of the real and of the refined structure (model). The deformations that provide the best matching between data and model are selected as principal strains at the atomic level.

The efficiency of the procedure can be optimized by suitable algorithms. For instance, the true volumetric deformation, computed by the VCD method, is exploited to decrease the number of degrees of freedom of the problem. In fact, one of the stretch ratios can be computed from the volumetric strain as:

$$\lambda_{vol} = \lambda_i \lambda_j \lambda_k \iff \lambda_i = \frac{\lambda_{vol}}{\lambda_j \lambda_k} \quad i \neq j \neq k \qquad (3)$$

Although computationally time consuming, the eVCD can be used with highly distorted structures or with atoms that are not fully coordinated, giving values of the principal strains comparable to the real ones.

3. RESULTS AND DISCUSSION

3.1. Isotropic and Anisotropic Strains

The deformation field in the atomistic models was characterized by the most significant isotropic and anisotropic tensor components. The local structure, surrounding each atomic position, was defined. Then, the principal strain tensor (ε_{I}, $\varepsilon_{\mathrm{II}}$ and $\varepsilon_{\mathrm{III}}$) and thus the volumetric and deviatoric components were computed by the following equations:[27]

$$\varepsilon_{vol} = \varepsilon_{\mathrm{I}} + \varepsilon_{\mathrm{II}} + \varepsilon_{\mathrm{III}} + \varepsilon_{\mathrm{I}}\varepsilon_{\mathrm{II}} + \varepsilon_{\mathrm{I}}\varepsilon_{\mathrm{III}} + \varepsilon_{\mathrm{II}}\varepsilon_{\mathrm{III}} + \varepsilon_{\mathrm{I}}\varepsilon_{\mathrm{II}}\varepsilon_{\mathrm{III}} \qquad (4)$$

$$\varepsilon_{dev} = \frac{2}{3}\sqrt{(\varepsilon_{\mathrm{I}} - \varepsilon_{\mathrm{II}})^2 + (\varepsilon_{\mathrm{I}} - \varepsilon_{\mathrm{III}})^2 + (\varepsilon_{\mathrm{II}} - \varepsilon_{\mathrm{III}})^2} \qquad (5)$$

The distribution of those two scalars were checked in the case of an elementary deformation field. A square parallelepiped cell was filled with a periodic *fcc* crystal structure; then, every atomic position was displaced accordingly to the local strain components (Fig. 3).

Periodical Boundaries Conditions (PBCs) were applied, achieving fully coordinate structures at each atomic position. That assumption allowed the CCD method to estimate the strain at the atomic level everywhere in the model. At the same time, the local detectable structures were geometrically affine to the reference crystal structure. The real and estimated local volumetric and deviatoric strain fields obtained with different computing methods, are shown in Figure 4.

RESEARCH ARTICLE

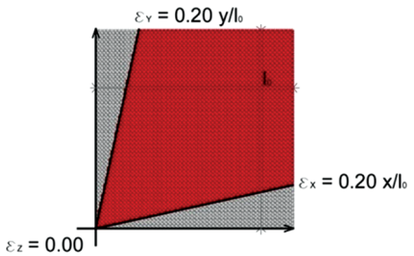

Fig. 3. Strain field diagrams in the square parallelepiped cell model.

The absolute values of the volumetric strain computed by all methods are close to the expected (true) ones. Only the weighted VmmCD method slightly changes the pattern of the strain field in a non-linear way. Conversely, the values of the deviatoric strain have a strong dependence on the computing method. Again, the CCD and the unweighted VmmCD methods gave results close to the real. The VCD and the weighted VmmCD methods are close, but the patterns are stretched and the absolute values are significantly different from the real ones. Moreover, if the local structure would be highly distorted or not fully coordinated, the CCD method would be unable to work. Also an unweighted VmmCD would be affected by an incomplete coordination.

The weighted VmmCD, the VCD and the eVCD methods can always be used, either in the core of the defects and through the grain boundaries in a polycrystalline microstructure. The mismatch of the deviatoric strain computed by those methods is due to the underlying assumptions and to their capability to assess the distortion of the crystallographic symmetries (Fig. 5). The assumption of the equivalent inertia of the parallelepiped solid in place of the real VC, which is employed in VCD method, could be replaced by more sophisticate functions. Further improvements are needed to fully solve the deformation at the atomic level through the VCD method.

3.2. Strain at the Atomic Level in a Nano-Polycrystalline Microstructure from MD

The strain at the atomic level was computed in the numerical model of an Al nano-polycrystalline microstructure using the discussed analysis methods and an *fcc* crystal structure as a reference (unit cell size of 4.04950 Å).

The deformation field was characterized in the microstructure equilibrated using the Embedded Atom Method potential, respectively after 1 ns and after 2.3 ns from the start of the simulation (Fig. 6). No significant differences were detected in the strain fields computed at the two equilibration times.[28] In particular, a Single Frame (SF) and the system Averaged over 150 Frames (AF) were investigated. Figure 7 shows the strain at the atomic level on a planar cross-section of the model at an equilibration time of 2.3 nano seconds.

It is quite evident that the CCD, as well as any method based on the crystallographic geometry, can provide results

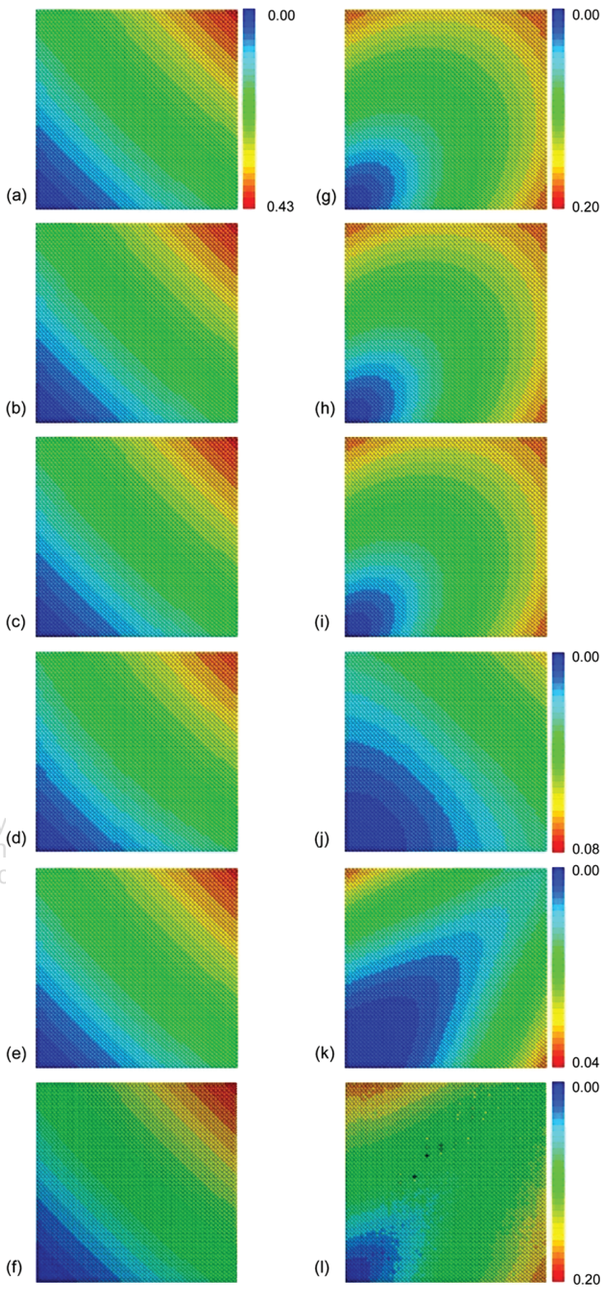

Fig. 4. Strain field computed by the applied deformation (a), (g) and estimated by several methods: CCD (b), (h), non-weighted VmmCD (c), (i), weighted VmmCD (d), (j), VCD (e), (k), eVCD (f), (l). The volumetric (a)–(f) and deviatoric (g)–(l) strain at the atomic level in the model are showed as the most significant deformation properties.

only in regions where atoms are fully coordinated and the local structure is not too much distorted. This condition is commonly not satisfied at the grain boundary, and in the core of the defects. Hence, only a fraction of the strain field can be investigated by CCD and gaps in the strain maps appear (white regions in Fig. 7). Moreover, a semi-stochastic fluctuation of the strain in the model, caused by

RESEARCH ARTICLE

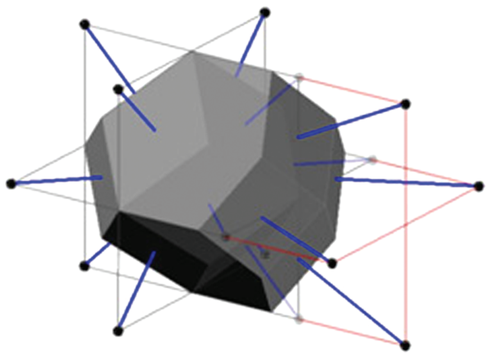

Fig. 5. Voronoi tessellations of a deformed *fcc* structure made by displacing uniformly the positions of a wall side.

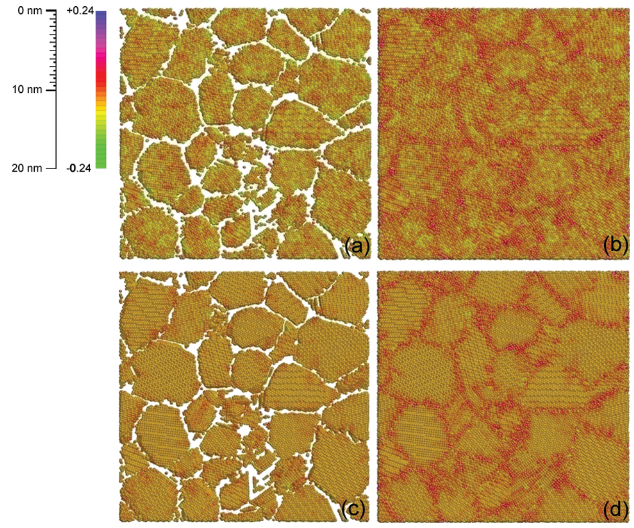

Fig. 7. Volumetric strain at the atomic level in a cross-section of the numerical model computed by CCD (a), (c) and VCD (b), (d) methods for the Single Frame (a), (b) and Averaged Frame (c), (d) cases.

the diffuse dynamic contribution, is clearly evident in the single frames and tend to be cancelled out in the model averaged over a long time period.

The VCD method, being unaffected by the local crystallography, is able to provide a strain value associated to each and all atomic positions. A smooth increase in local strain close to the boundaries appears in Figure 7. The boundary embodies several local distorted configurations, allowing the structures of neighbour grains to be joined together. The quick increase of the strain intensity near the grain boundaries is due to the small dimensions of the grains (about 6 nm), causing a steep change from core to boundary regions.

Figure 8 shows the volumetric strain distributions for the whole cluster computed using the CCD and VCD methods on the single and on the averaged frame. Accounting for the intense deformation at the grain boundary has a dramatic effect on the distribution of the local strain over the whole cluster. The asymmetry in the distributions is caused by the overlapping of the contributions from core and boundary regions. The time average (AF) leads to sharper distributions as the smearing effect of the dynamic contributions is removed. Again, the semi-stochastic nature of the local deformation due to the thermal movement leads to more symmetric distribution functions.

The deviatoric strain is more deeply affected by the dynamic contribution than the volumetric strain (cf. Fig. 9). In SF, the local structure is constantly distorted due to the thermal movement. The time dependent distortion is removed by the average of a suitable sequence of frames. The more uniform behaviour of the atoms in the core of the grains allows the averaged local structure to be less affected by a spread anisotropic deformation. Hence,

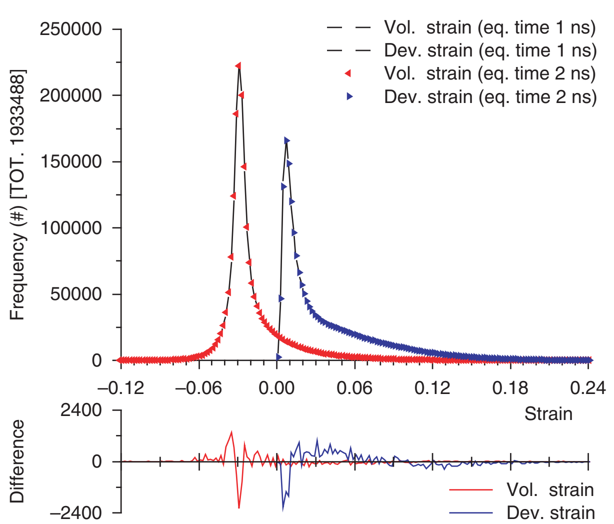

Fig. 6. Frequency distributions of the local volumetric (red) and deviatoric (blue) strain in the numerical model computed by the VCD method for Averaged Frame after 1 ns (void dots) and 2.3 ns (full dots) as equilibration time.

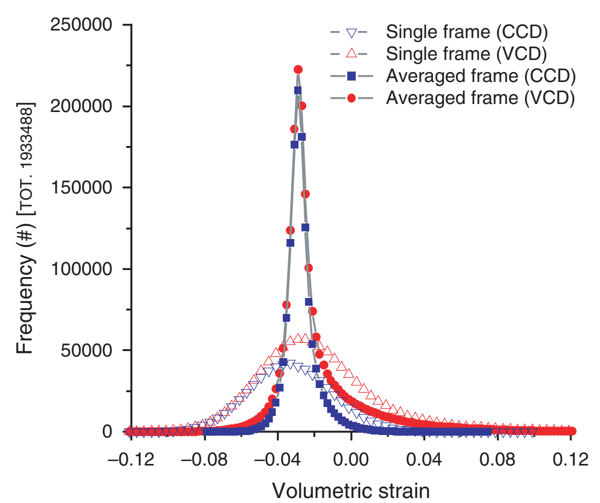

Fig. 8. Frequency distributions of the local volumetric strain in the numerical model computed by CCD (blue dots) and VCD (red dots) methods for the Single Frame (open symbols) and Averaged Frame (full symbols) cases.

RESEARCH ARTICLE

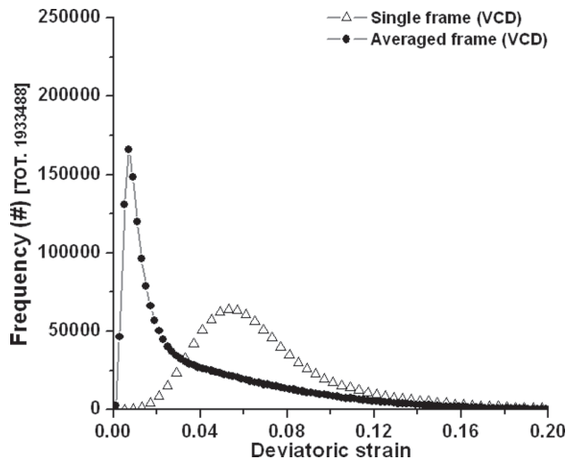

Fig. 9. Frequency distributions of the local deviatoric strain in the numerical model computed by VCD method for the Single Frame (open symbol) and Averaged Frame (full symbol) cases.

a strong asymmetry in the distribution of the deviatoric strain can be linked to a difference in behaviour of core versus boundary. This pronounced difference allows us to clearly identify the boundary region.

Figure 10 shows the distribution of the volumetric and deviatoric strains at the atomic level associated to the local crystalline symmetry. The latter was defined as:

(i) the number of missing neighbours in the case coordination is less than 12;

(ii) the number of contiguous shells having fully coordinated neighbours in the case of fully coordinated position.

An inverse correlation is found between the local crystalline symmetry and the variance of the distributions, for both the volumetric and deviatoric components. A sharp discontinuity in the trends appears when crossing the condition of full coordination. While the position of the volumetric strain distribution is weekly dependent on the local crystalline symmetry, the deviatoric distribution tends to shift to higher strains for decreasing coordination.

The three principal types of strain in the system (usually quoted when dealing with stress and diffraction[29]) can be clearly identified from the mean volumetric and deviatoric strain computed along a line section in the model (Fig. 11). An isotropic compression of 0.030 and anisotropic components of 0.005 are found as the I type of the local strain in AF model. The type II and type III of both the volumetric and the deviatoric strains are close to zero. In the case of the SF model a significantly broader strain fluctuation

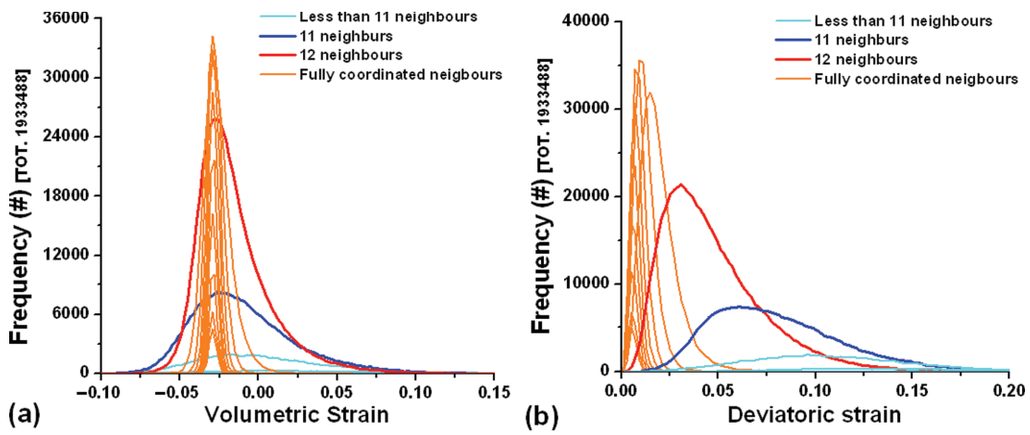

Fig. 10. Frequency distributions of the local volumetric (a) and deviatoric (b) strains in the numerical model computed by VCD for the Averaged Frame referred to the local crystalline symmetry (see text for details).

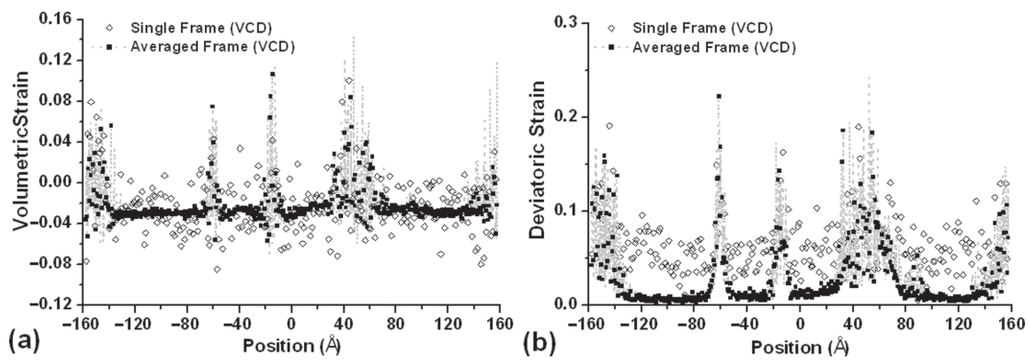

Fig. 11. Volumetric (a) and deviatoric (b) strain at the atomic level along a line section through the cluster.

RESEARCH ARTICLE

appears. This feature hides the marked changes in the strain intensity close to the defects, rendering more difficult to correctly identify the boundary regions. In AF, however, the transition from the core to the boundary zones is clear and extremely sharp. Moreover, the deviatoric strain in the SF model and in the AF model shown an evident gap due to the dynamic component. This behaviour further confirms the intrinsic isotropic deformation of the crystallographic structures in the core of the grains. Hence, when a time average computation is employed, the anisotropic contribution in the grain cores tends to disappear.

4. CONCLUSION

A new method has been presented for computing the strain at the atomic level. Grouped under the name of Voronoi Cell Deformation (VCD), the different forms of the proposed algorithm are all based on a Voronoi Tessellation to identify the local atomic arrangement. The principal stretch ratios are computed from the differences of the inertia between the real and a reference configuration, also considering a uniform or a concentrated distribution of mass. The use of tessellation allows strains to be computed also in the grain boundary regions where traditional methods based on the local crystallography cannot be used.

The VCD was compared with the known CCD method for the analysis of a simulated nano-polycrystalline microstructure. Contrary to the CCD, which does not allow highly distorted regions to be considered, the VCD is able to provide information in any point in the cluster. A marked difference in behaviour is detected in the grains between core and boundary. A distribution of the strain with large changes at the interface between grains is shown by studying the strain along linear sections in the cluster. Differences between the results of CCD and VCD are as expected, as the latter considers all atoms, including those in highly deformed positions, as in the grain boundary regions.

APPENDIX A

Deformation of Convex Polyhedra from Volume Properties

The deformation of a convex polyhedron is proportional to the change in the geometric properties such as the moments of volume. The latter are easily computed e.g., by the equations proposed by Tuzikov et al.[30] In particular, as the VCs are convex polyhedra (bound by polygonal faces), they can be decomposed into tetrahedra that divide the faces into triangles (Fig. 12).

If we define the matrix:

$$\mathbf{A} = \begin{pmatrix} a_1 & b_1 & c_1 \\ a_2 & b_2 & c_2 \\ a_3 & b_3 & c_3 \end{pmatrix} \tag{6}$$

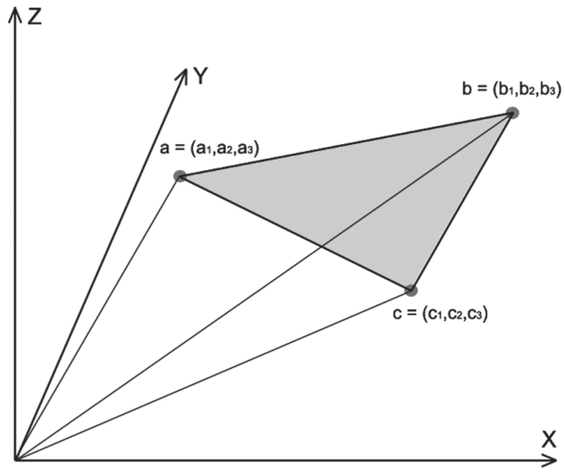

Fig. 12. Geometric description of a tetrahedron in space.

we can calculate the moment of mass of the whole polyhedron P:

$$m_{P,str} = \sum_T m_{T,str} \tag{7}$$

in terms of the moments of mass of the N composing tetrahedra T:

$$m_{T,str} = \int_T (x_i^s x_j^t x_k^r)\, dx_i\, dx_j\, dx_k \qquad i,j,k = 1,\ldots,3 \;\; i \neq j \neq k \tag{8}$$

Just three moments of mass for each tetrahedron:

$$m_{T,100} = \frac{1}{24}|\mathbf{A}|(a_1 + b_1 + c_1) \tag{9}$$

$$m_{T,101} = \frac{1}{120}|\mathbf{A}|(2a_1a_3 + a_1b_3 + a_1c_3 + a_3b + 2b_1b_3 + b_1c_3 + c_1a_3 + c_1b_3 + 2c_1c_3) \tag{10}$$

$$m_{T,200} = \frac{1}{60}|\mathbf{A}|(a_1^2 + b_1^2 + c_1^2 + a_1b_1 + a_1c_1 + b_1c_1) \tag{11}$$

suffice to calculate the whole moment of inertia tensor I_P:

$$\mathbf{I}_P = \begin{pmatrix} m_{P,020}+m_{P,002} & -m_{P,110} & -m_{P,101} \\ -m_{P,110} & m_{P,200}+m_{P,002} & -m_{P,110} \\ -m_{P,101} & -m_{P,110} & m_{P,200}+m_{P,020} \end{pmatrix} \tag{12}$$

The principal moments and directions of inertia can be then computed as the eigenvalues and eigenvectors of I_P:

$$\mathbf{I}_P^0 = \begin{pmatrix} I_{ii} & 0 & 0 \\ 0 & I_{jj} & 0 \\ 0 & 0 & I_{kk} \end{pmatrix} \tag{13}$$

Linking the inertia values of the VCs to the equivalent parallelepiped solids, the three positive stretch ratios are fully defined by the equations:

$$\lambda_n = \frac{L_{F,n}}{L_{0,n}} \;\Leftrightarrow\; x_{F,n} = \lambda_n x_{0,n} \quad n = i,j,k \tag{14}$$

$$J_{kk} = (I_{ii} + I_{jj} - I_{kk})/2 = \frac{x_i x_j x_k^3}{12} \tag{15}$$

$$\frac{J_{F,kk}}{J_{0,kk}} = \frac{x_{F,i} x_{F\,j} x_{F,k}^3}{12} \frac{12}{x_{0,i} x_{0,j} x_{0,k}^3}$$
$$= \frac{(x_{0,i} x_{0,j} x_{0,k}^3)\lambda_i \lambda_j \lambda_k^3}{(x_{0,i} x_{0,j} x_{0,k}^3)} = \lambda_i \lambda_j \lambda_k^3 \tag{16}$$

$$\lambda_k = \left[\left(\frac{J_{F,kk}}{J_{0,kk}} \right)^4 \Big/ \left(\frac{J_{F,ii} J_{F,jj}}{J_{0,ii} J_{0,jj}} \right) \right]^{1/10} \tag{17}$$

where L_F and L_0 are the final (F) and initial (0) lengths, respectively.

APPENDIX B

Deformation of Convex Polyhedra from Mass Properties

When concentrated masses are considered, Eq. (7) is replaced by:

$$m_{P,str} = \sum_T w_T x_i^s x_j^t x_k^r \tag{18}$$

where $w_T = S_T/S_P$ or $w_T = 1$ for the weighted and unweighted VmmCD, respectively. The term S_T is the surface area of the face of tetrahedron T shared with the polyhedron P, whereas S_P is the total surface area of the polyhedron.

The stretch ratios along the principal directions can be directly computed without any additional assumption from the principal inertia of the deformed and reference structures:

$$\lambda_k = \left[\frac{I_{F,ii} + I_{F,jj} - I_{F,kk}}{I_{0,ii} + I_{0,jj} - I_{0,kk}} \right]^{1/2} \tag{19}$$

References and Notes

1. P. M. Derlet, S. Van Petegem, and H. Van Swygenhoven, *Phys. Rev. B* 71, 024114 (**2005**).
2. D. Gross and M. Li, *Appl. Phys. Lett.* 80, 746 (**2002**).
3. T. Suzudo and H. Kaburaki, *Phys. Lett. A* 373, 4484 (**2009**).
4. D. Jang and M. Atzmon, *J. Appl. Phys.* 99, 083504 (**2006**).
5. A. Cao, *Mater. Sci. Forum* 633–634, 31 (**2010**).
6. H. Van Swygenhoven, D. Farkas, and A. Caro, *Phys. Rev. B* 62, 831 (**2000**).
7. Q.-K. Li and M. Li, *Appl. Phys. Lett.* 88, 241903 (**2006**).
8. G. J. Ackland and A. P. Jones, *Phys. Rev. B* 73, 054104 (**2006**).
9. D. J. Honeycutt and H. C. Anderson, *Phys. Rev. B* 91, 4950 (**1987**).
10. M. Samaras, P. M. Derlet, and H. Van Swygenhoven, *Phys. Rev. B* 68, 224111 (**2003**).
11. P. M. Derlet and H. Van Swygenhoven, *Phys. Rev. B* 67, 014202 (**2003**).
12. P. M. Derlet and H. Van Swygenhoven, *SRMS5? Conference*, Chicago (**2006**).
13. A. Stukowski, J. Markmann, J. Weissmüller, and K. Albe, *Acta Mater.* 57, 1648 (**2009**).
14. A. Leonardi, K. Beyerlein, T. Xu, M. Li, M. Leoni, and P. Scardi, *Zeitschrift für Kristallographie* (**2011**), in press.
15. S. Kumar, S. K. Kurtz, J. R. Banavar, and M. G. Sharma, *J. Stat. Phys.* 67, 523 (**1992**).
16. V. Lucarini, *J. Stat. Phys.* 130, 1047 (**2008**).
17. V. Lucarini, *J.Stat. Phys.* 134, 185 (**2009**).
18. T. Xu and M. Li, *Philos. Mag.* 89, 349 (**2009**).
19. T. Xu and M. Li, *Philos. Mag.* 90, 2191 (**2010**).
20. S. J. Plimpton, *J. Comput. Phys.* 117, 1 (**1995**).
21. M. S. Daw and M. I. Baskes, *Phys. Rev. B* 29, 6443 (**1984**).
22. K. W. Jacobsen, J. K. Nøskov, and M. J. Puska, *Phys. Rev. B* 35, 7423 (**1987**).
23. A. Hasnaoui, H. Van Swygenhoven, and P. M. Derlet, *Phys. Rev. B* 66, 184112 (**2002**).
24. J. Li and F. Shimizu, *Least-Square Atomic Strain* (**2005**), Unpublished.
25. P. H. Mott, A. S. Argon, and U. W. Suter, *J. Comput. Phys.* 101, 140 (**1992**).
26. M. O'Keeffe, *Acta Crystallogr. A* 35, 772 (**1979**).
27. A. Godeke, B. ten Haken, and H. H. J. Ten Kate, *Physica C* 372–376, 1295 (**2002**).
28. H. Van Swygenhoven, *Science* 5, 296 (**2002**).
29. P. J. Withers and H. K. D. H. Bhadeshia, *Mater. Sci. Technol.* 17, 355 (**2001**).
30. A. V. Tuzikov, S. A. Sheynin, and P. V. Vasiliev, *Pattern Recognition* 36, 2521 (**2003**).

Received: 5 July 2011. Accepted: 14 November 2011.